Applied Catalysis B: Environmental 164 (2015) 77–81

Contents lists available at ScienceDirect

Applied Catalysis B: Environmental

journal homepage: www.elsevier.com/locate/apcatb

# Enhanced catalytic activity of potassium-doped graphitic carbon nitride induced by lower valence position

Mo Zhang, Xiaojuan Bai, Di Liu, Jun Wang, Yongfa Zhu*

*Department of Chemistry, Beijing Key Laboratory for Analytical Methods and Instrumentation, Tsinghua University, Beijing 100084, China*

ARTICLE INFO

*Article history:*
Received 2 July 2014
Received in revised form 3 September 2014
Accepted 5 September 2014
Available online 16 September 2014

*Keywords:*
g-$C_3N_4$
Potassium doping
Photocatalysis
Phenol degradation

ABSTRACT

The potassium doped graphitic carbon nitride (K-$C_3N_4$) photocatalysts were prepared via thermal polymerization of dicyandiamide and KI in atmosphere. The valence band (VB) position of g-$C_3N_4$ was decreased via potassium doping, resulting in enhanced separation and immigration of photogenerated carriers under visible light. The optimum K-$C_3N_4$ exhibited obviously enhanced photocatalytic activities for phenol and MB degradation, which were about 3.3 and 5.8 times as high as those of bulk g-$C_3N_4$, respectively. The photocatalytic activity of K-$C_3N_4$ decreased with excessive KI mass fraction in the precursor due to the incomplete polymerization of g-$C_3N_4$.



## 1. Introduction

Photocatalysis is regarded as a promising technique to deal with the problems of resources and environment [1–5]. Graphitic carbon nitride (g-$C_3N_4$) has been widely applied in water decomposition, oxygen reduction, organic photosynthesis and environmental remediation, due to its visible light activity and chemical stability [6–8]. However, its photocatalytic degradation ability of organic pollutants, especially benzene-based organics, is seriously limited by its low catalytic activity and ring opening ability due to the high valence band (VB) position [9]. In addition, the fast charge recombination is another drawback to limit the photocatalytic activity [10,11]. Hence, the development of g-$C_3N_4$ with lower VB position, considerable catalytic activity and enhanced charge separation and immigration has become an urgent necessity.

Among all the strategies to enhance the activity of photocatalysts, doping is one of the most intensively researched methods [12–16]. Nonmetal doping can increase the visible light absorption, modify the carrier mobility of catalysts and modulate the electronic structure of catalysts [11,17]. Phosphorus doped g-$C_3N_4$ can provided a much better electric (dark) conductivity and an improved photocurrent [11]. Sulfur doped graphitic $C_3N_4$ ($C_3N_{4-x}S_x$) is reported to display increased valence bandwidth and elevated conduction band minimum [18]. However, the valence position of the catalysts is difficult to decrease by nonmetal, which may limit their application in organic pollutants degradation. Alkali doping can modulate the electronic structure of materials, which may change the performance of the catalysts [19,20]. In consideration of the drawbacks of fast charge recombination, high VB position, low catalytic activity and ring opening ability of g-$C_3N_4$, alkali doping may modulate the electronic structure and promote the catalytic activity of g-$C_3N_4$. $C_3N_4$-based intercalated compound with alkali metals can induce the non-uniform spatial charge distribution and enhance the separation efficiency of photogenerated carriers [21]. In addition, potassium-modified g-$C_3N_4$ can effectively reduce the recombination rate of photogenerated electron–hole pairs and shows high photocatalytic for hydrogen evolution [22]. Although alkali metals doped g-$C_3N_4$ has been researched, g-$C_3N_4$ with modulate electronic structure and catalytic activity for organic pollutants degradation is rarely realized by alkali doping.

Herein, potassium is chosen as dopant into g-$C_3N_4$ to demonstrate the conception above. The valence band position of g-$C_3N_4$ shifted to a lower energy position via potassium doping. The photocatalytic activities of K-$C_3N_4$ were about 3.3 and 5.8 times as high as those of bulk g-$C_3N_4$ for phenol and MB degradation, which can ascribe to the decreased valence position and the enhanced separation and immigration of photogenerated carriers under visible light. This work provides a simple and low-cost method to synthesize the doping catalyst, which shed light on great potentials for application in treatment of environmental pollution.

* Corresponding author. Tel.: +86 10 6278 3586; fax: +86 10 6278 7601.
*E-mail address:* zhuyf@mail.tsinghua.edu.cn (Y. Zhu).

http://dx.doi.org/10.1016/j.apcatb.2014.09.020
0926-3373/

## 2. Experimental

### 2.1. Synthesis of photocatalyst

Dicyandiamide was purchased from Sinopharm Chemical Reagent Corp, PR China. All other reagents used in this research were analytically pure and used without further purification.

The K-$C_3N_4$ photocatalysts were prepared by thermal polymerization of dicyandiamide and KI in atmosphere. The typical preparation of K-g-$C_3N_4$ photocatalysts was as follows: 5 g of dicyandiamide and KI was put in a Muffle Furnace and heated to 550 °C for 4 h to complete the reaction. The yellow products were washed with nitric acid (0.1 mol $L^{-1}$) and deionized water to remove the residue adsorbed on the surface of g-$C_3N_4$. Then the pure products were dried at 80 °C for 12 h.

### 2.2. Characterizations

The morphologies and structures of the samples were examined with HITACHI HT7700 transmission electron microscopy (TEM) operated at an accelerating voltage of 100 kV. UV–vis diffuse reflectance spectroscopy (DRS) was carried out on a Hitachi U-3010 UV-vis Spectrophotometer using $BaSO_4$ as the reference. The crystallinity of the as-prepared sample was characterized by X-ray diffraction (XRD) on Bruker D8-advance diffractometer using Cu-Kα radiation (λ = 1.5418 Å). The photocurrents were measured on an electrochemical system (CHI 660D, China). Raman spectra were obtained by using a HORIBA JY HR800 confocal microscope Raman spectrometer employing an Ar-ion laser (633 nm). A 50× telephoto Olympus objective lens was used to focus the laser on the samples. All spectra were calibrated with respect to silicon wafer at 520.7 $cm^{-1}$. Fourier transformed infrared (FTIR) spectra were recorded on a Bruker VERTEX 700 Spectrometer. Photoluminescence spectra (PL) of the samples were obtained at room temperature using a HORIBA Aqualog Fluorescence Spectrometer.

### 2.3. Photocatalytic experiments

The photocatalytic activities were evaluated by the decomposition of phenol under visible light irradiation (λ > 420 nm) and simulated sunlight irradiation. Visible irradiation was obtained from a 500 W Xe lamp (Institute for Electric Light Sources, Beijing) with a 420 nm cutoff filter, and the average visible light intensity was 35 mW $cm^{-2}$. For the photocatalytic experiments, 25 mg of photocatalyst was totally dispersed in an aqueous solution of phenol (50 mL, 5 ppm). Before irradiation, the suspensions were magnetically stirred in the dark for 2 h to get absorption–desorption equilibrium between the photocatalyst and phenol. At certain time intervals, 3 mL aliquots were sampled and centrifuged to remove the particles. The concentration of phenol was analyzed by chromatographic experiments with HPLC–UV/vis system.

### 2.4. Analyses of the degradation intermediates for phenol

The chromatographic experiments with HPLC–UV/vis system were carried out using an ultraviolet absorbance detector (K 2501) operated at 275 nm phenol coupled to a Venusil XBP-C18 (Agela Technologies Inc.) column. Before the analysis, the samples were filtered through millipore discs of 0.45 μm to protect the chromatographic column. The mobile phase used for eluting phenol and its degradation intermediates from the HPLC columns consisted of methanol and water (60:40, v/v) at a flow rate of 1 mL $min^{-1}$.

**Table 1**
The concentrations of elements for different materials determined by XRF.

| Materials | N | C | O | K | I |
|---|---|---|---|---|---|
| Pure $C_3N_4$ | 68.89% | 29.05% | 1.41% | 0 | 0 |
| 10%-K-g-$C_3N_4$ | 65.08% | 27.61% | 1.93% | 4.58% | 0.72% |
| 16%-K-g-$C_3N_4$ | 64.37% | 27.95% | 2.12% | 4.93% | 0.59% |
| 22%-K-g-$C_3N_4$ | 63.69% | 27.81% | 2.61% | 5.47% | 0.35% |
| 27%-K-g-$C_3N_4$ | 62.81% | 28.31% | 2.85% | 5.66% | 0.30% |
| 30%-K-g-$C_3N_4$ | 63.69% | 28.14% | 3.28% | 4.58% | 0.20% |

### 2.5. Photoelectrochemical measurements

To investigate the transition of photogenerated electrons of K-g-$C_3N_4$, a standard three-electrode cell with a working electrode (as-prepared photocatalyst, a platinum wire as counter electrode, and a saturated calomel electrode (SCE) as reference electrode were used in the photoelectric studies. 0.1 M $Na_2SO_4$ was used as the electrolyte solution. Potentials are given with reference to the SCE. The photoresponses of the photocatalysts as light on and off were measured at 0.0 V. The working electrodes were prepared as follows: 5 mg of the as-prepared photocatalyst was suspended in 1 mL water to produce slurry, which was then dip-coated onto a 2 cm × 4 cm indium tin oxide (ITO) glass electrode. Electrodes were exposed to air atmosphere for 12 h to eliminate water and subsequently calcined at 200 °C for 5 h.

## 3. Results and discussions

The concentrations of elements for different materials are explored by X-ray fluorescence spectroscopy (XRF). As shown in Table 1, the potassium concentration increases with the increasing KI content in the precursor with mass fraction of KI from 0% to 27%. The decreased potassium concentration of 30%-K-$C_3N_4$ may be ascribed to the incomplete polymerization of dicyandiamide with excessive KI. When the KI mass fraction is cross the threshold of 27%, the contact area between K and dicyandiamide is decreased and the most of the KI tends to thermal decompose instead of react with dicyandiamide. The chemical states of potassium were revealed by measuring K 2p levels using XPS. The K2p peaks of 22%-K-$C_3N_4$ are explored by peak separation (Fig. 1). The K2p3/2 and K2p1/2 peaks for 22%-K-$C_3N_4$ are discovered at 292.8 and 295.3 eV, which are lower than potassium salt [23]. Interestingly, the peak locations of K2p3/2 and K2p1/2 for K-$C_3N_4$ are increased with increasing KI content in the precursor (Fig. S1), indicating the existent of covalent bond between K and $C_3N_4$.

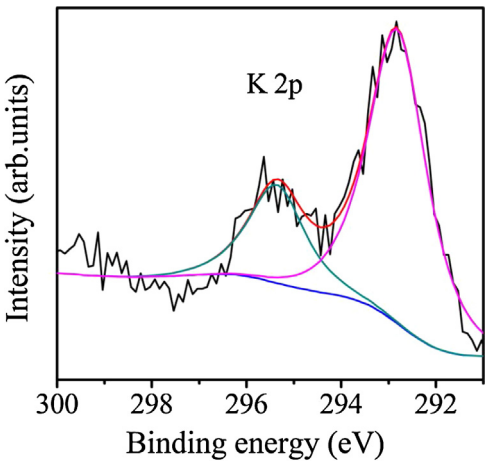


**Fig. 1.** The K2p XPS spectrum of 22%-K-$C_3N_4$.

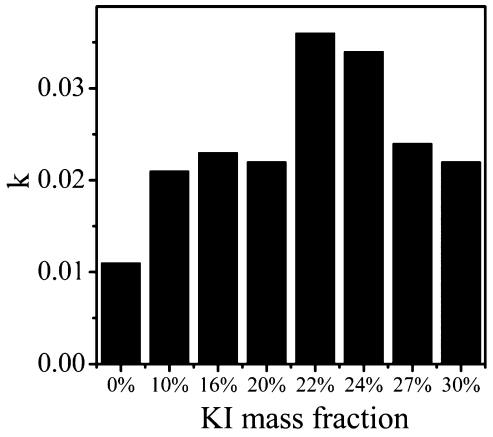


**Fig. 2.** The apparent rate constants of photocatalytic degradation of phenol over pure g-$C_3N_4$ and K-$C_3N_4$ with different KI mass fraction under visible light irradiation ($\lambda > 420$ nm).

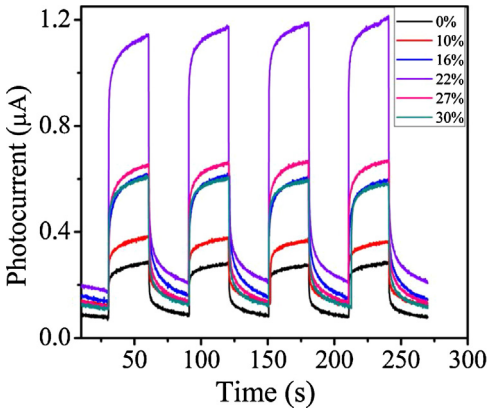


**Fig. 3.** Photoresponses of pure g-$C_3N_4$ and K-$C_3N_4$ with different KI mass fraction under visible light irradiation ($\lambda > 420$ nm, [$Na_2SO_4$] = 0.1 M).

The K-$C_3N_4$ photocatalysts were prepared via thermal polymerization of dicyandiamide and KI in atmosphere. The TEM images of 22%-K-$C_3N_4$ and pure g-$C_3N_4$ (Fig. S2) show both of them exhibit bulk morphology, indicating that the morphology of K-$C_3N_4$ has not appreciably changed by K doping. Figs. 2 and S3 show the photocatalytic activity of $C_3N_4$ and K-$C_3N_4$ photocatalysts for phenol degradation with different mass fraction of KI in the precursor. The photocatalytic rate constant is obviously enhanced with increasing KI content. When the mass fraction of KI reaches 22%, the apparent rate constant k is almost 3.3 times as high as that of pure $C_3N_4$. However, as the proportion of KI further increases, the degradation rate decreases gradually though it remains higher than that of $C_3N_4$. This change in photocatalytic activity of K-$C_3N_4$ may be attributed to the balance between the enhancement and defects caused by potassium doping. Although K doping is beneficial for photocatalytic activity, it will influence on the polymerization at too much addition. The excess KI may prevent dicyandiamide from polymerization and lead to the defects and decreased polymerization degree of K-$C_3N_4$. The K-$C_3N_4$ also exhibited enhanced photocatalytic activities for MB degradation, which was about 5.8 times as high as those of bulk g-$C_3N_4$ (Fig. S4).

Photocurrents are measured for K-$C_3N_4$ and $C_3N_4$ electrodes to investigate the transmission of photogenerated carriers (Fig. 3). Under visible light irradiation, the photocurrent is remarkably enhanced along with the increase of KI content. The photocurrent of 22%-K-$C_3N_4$ is about four times as high as that of the pure $C_3N_4$ electrode, indicating the enhanced separation and transition efficiency of photoinduced electrons and holes. The photocurrent is decreased when the mass fraction of KI further increases, which was in agreement with the change of the photocatalytic activity. Brunauer–Emmett–Teller (BET) measurements (Fig. S5) reveals the surface areas of K-$C_3N_4$ decreased from 10.5 to 3.5 with increased mass fraction of KI. The decreased BET surface areas may related to the agglomerate of K-$C_3N_4$ during thermal polymerization, indicating the enhanced catalytic activity is not associated with the specific surface areas of K-$C_3N_4$.

The photodegradation intermediates is investigated by chromatograms of phenol before and after photocatalytic degradation for 4 h monitored at 275 nm (Fig. S6). The intensity of phenol (5.3 min) was decreased with constant visible light irradiation. The new peaks at lower retention times can be ascribed to the intermediates of phenol, such as dihydroxybenzene, 4,4-dihydroxybiphenyl and maleic anhydride [9,24–26]. The higher intensity of intermediates by K-$C_3N_4$ than pure $C_3N_4$ indicates that the catalytic activity of K-$C_3N_4$ is remarkable enhanced.

The FTIR spectra of the K-$C_3N_4$ exhibit the same bands as pure $C_3N_4$ expect a band at 2177 $cm^{-1}$ (Fig. 4), corresponding to the defects of cyano group stretch caused by the incomplete polymerization and the loss of ammonia [21]. The XRD patterns (Fig. 5) indicate the crystal phase of $C_3N_4$ does not change with K doping. However, the overall diffraction intensity is much weakened, which can be attribute to the defects caused by the incomplete polymerization. The typical D band at 1360 $cm^{-1}$ and G band at 1553 $cm^{-1}$ for g-$C_3N_4$ in the Raman spectrum are referred to the disorder in graphite and the in-plane bond-stretching motion of pairs of C sp2 atoms [27] (Fig. 6). With the increase of KI content in the precursor,

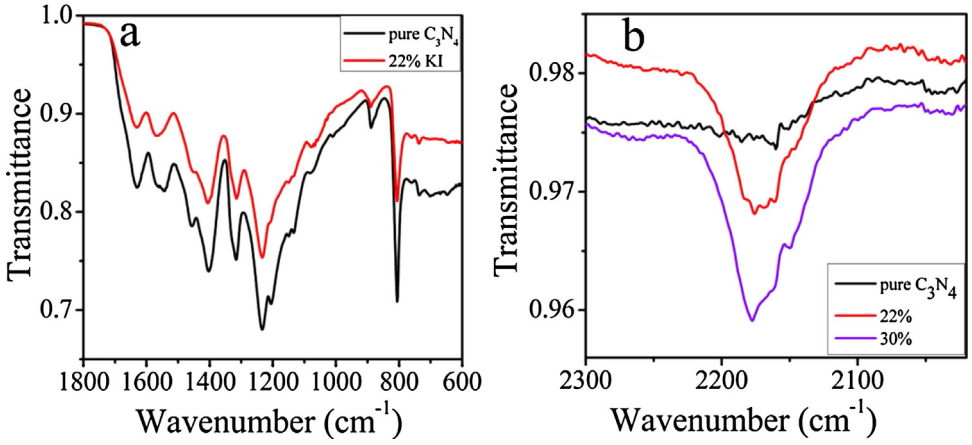


**Fig. 4.** IR spectra of g-$C_3N_4$ and K-$C_3N_4$ with different KI mass fraction (22% and 30%).

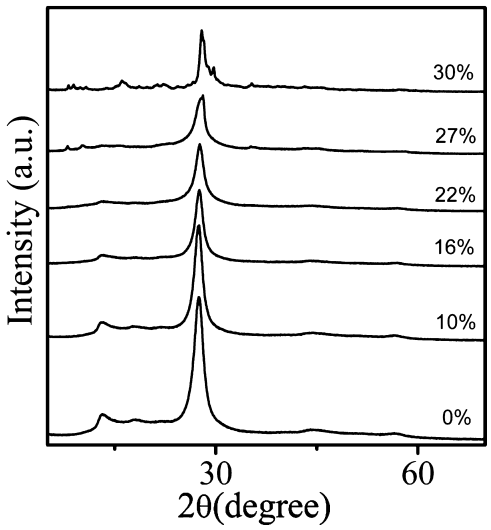


**Fig. 5.** XRD spectra of pure g-$C_3N_4$ and K-$C_3N_4$ with different KI mass fraction.

the emergency of several vibration modes at 737 $cm^{-1}$, 980 $cm^{-1}$, 1110 $cm^{-1}$, 1170 $cm^{-1}$, 1227 $cm^{-1}$, 1330 $cm^{-1}$ and 1586 $cm^{-1}$ are observed which can be attribute to melem [28]. The results indicate that the chemical structures of K-$C_3N_4$ photocatalysts were not changed by K doping. However, the excess KI may prevent dicyandiamide from polymerization, lead to the defects and decreased polymerization degree of K-$C_3N_4$.

As shown in Fig. 7, the smaller arc radius on the electrochemical impedance spectroscopy (EIS) Nyquist plots of K-$C_3N_4$ with increased KI content under visible light irradiation indicate that the separation and transmission efficiency of photogenerated electron–hole pairs are obviously enhanced. The arc radius on the EIS Nyquist plot of K-$C_3N_4$ was also smaller than that of $C_3N_4$ without irradiation, suggesting that K doping changed the charge distribution of $C_3N_4$ and made charge transfer easier [29]. In addition, the photoluminescence (PL) intensity of 22%-K-$C_3N_4$ (Fig. 8) declines substantially compared with pure $C_3N_4$, indicating that the relaxation of a fraction of K-$C_3N_4$ excitons may occur via other

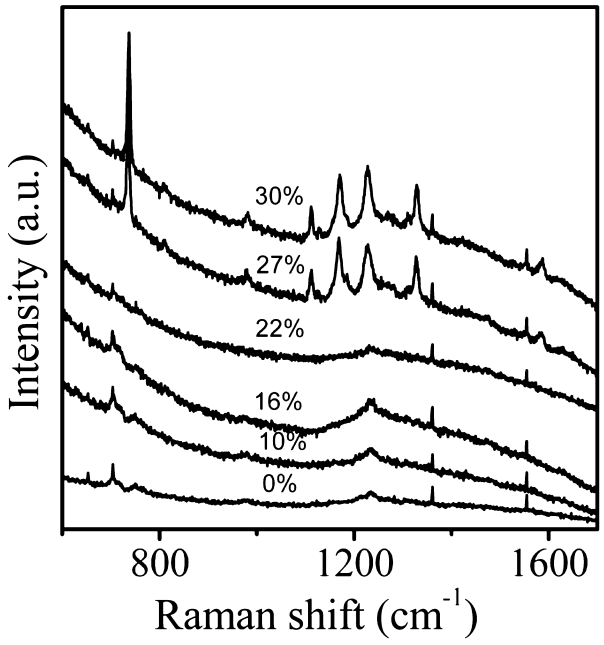


**Fig. 6.** Raman spectra of g-$C_3N_4$ and K-$C_3N_4$ materials.

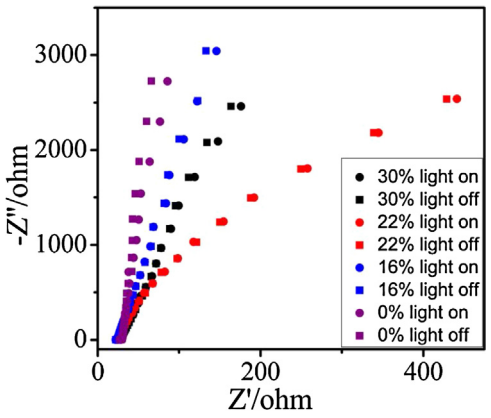


**Fig. 7.** EIS Nyquist plots of pure g-$C_3N_4$ and K-$C_3N_4$ with different KI mass fraction.

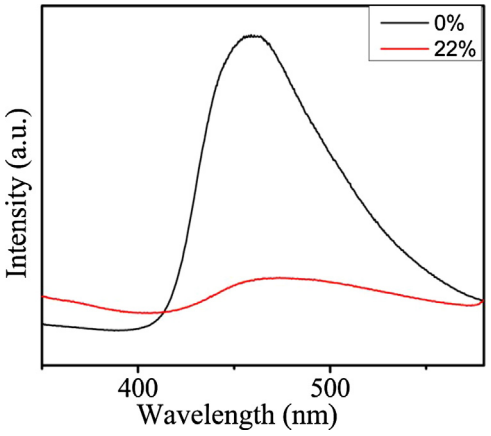


**Fig. 8.** Photoluminescence (PL) spectra of pure g-$C_3N_4$ (0%) and 22%-K-$C_3N_4$.

way instead of radiative paths [10,30]. Thus, the lower recombination probability of photogenerated charge carriers for K-$C_3N_4$ compared to pure $C_3N_4$ can be inferred. This result implied that K doping could obviously favor the separation and transition of photogenerated carriers in K-$C_3N_4$ photocatalysts and enhanced the photocatalytic activity.

The enhanced mineralization ability and photocatalytic activity of K-$C_3N_4$ is related to the changed electronic structures of K-$C_3N_4$. The UV–vis DRS spectra (Fig. 9) indicate that the intrinsic absorption edge of $C_3N_4$ shows a little red-shift upon potassium doping. The bandgaps of $C_3N_4$ and 22%-K-$C_3N_4$ determined are 2.67 and

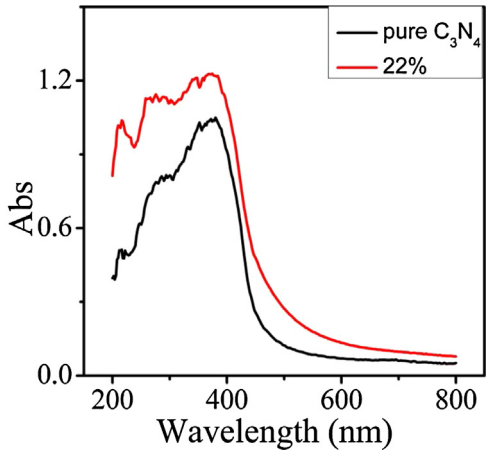


**Fig. 9.** UV–vis diffuse reflectance spectra of pure g-$C_3N_4$ and 22%-K-$C_3N_4$.

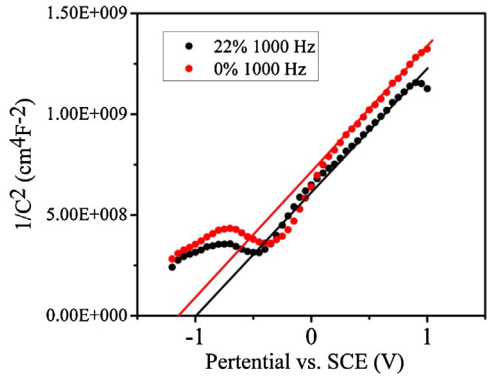


**Fig. 10.** Mott–Schottky (MS) plots of pure $C_3N_4$ and 22%-K-$C_3N_4$ film electrodes at a frequency of 10 and 100 Hz in an aqueous solution of $Na_2SO_4$ (0.1 M).

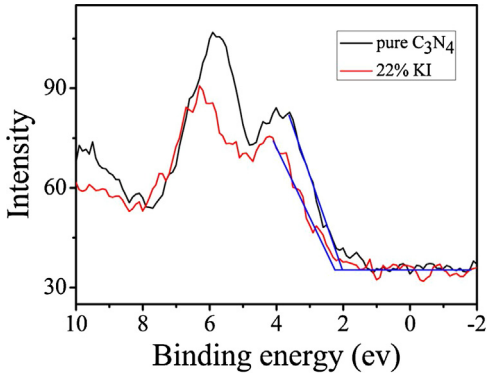


**Fig. 11.** The valence band spectra of X-ray photoelectron spectroscopy for pure $C_3N_4$ and 22%-K-$C_3N_4$.

2.64 eV. The electronic structures of $C_3N_4$ and 22%-K-$C_3N_4$ are estimated by their flat-band potentials [31,32]. The calculated flat band potential ($V_{fb}$) for $C_3N_4$ and 22%-K-$C_3N_4$ electrodes are −1.15 and −0.99 V versus SCE (Fig. 10), respectively. The conducted band (CB) position is close to the flat-band potential, and the valence band (VB) position can be estimated by the CB and band gap energy. The CB and VB of pure $C_3N_4$ are similar to the results of density functional theory calculations [7]. While the bandgap energy of 22%-K-$C_3N_4$ is nearly the same as that of pure $C_3N_4$, the flat-band potential of 22%-K-$C_3N_4$ is upshifted by 0.2 V. Thus, the potassium doping might cause an anodic shift of the valence band edge of $C_3N_4$, which consequently results in its enhanced degradation ability of organic pollutants.

X-ray photoemission spectroscopy (XPS) is a powerful tool to study the electronic structure of solids [33]. The electronic structures of $C_3N_4$ and K-$C_3N_4$ are investigated by valence band spectra of X-ray photoelectron spectroscopy. As shown in the valence band spectra (Fig. 11), the valence-band electronic structure of pure $C_3N_4$ is in reasonable agreement with the calculations. The valence-band position of K-$C_3N_4$ is decreased compared with pure $C_3N_4$, which is also similar to the results of flat band potential. The results indicate that the electronic structure of g-$C_3N_4$ is changed by K doping. The decreased valence position of K-$C_3N_4$ leads to its enhanced degradation ability of organic pollutants.

## 4. Conclusion

The K doped $C_3N_4$ photocatalysts were prepared via in situ calcination method in atmosphere. The K-$C_3N_4$ exhibited obviously enhanced photocatalytic activities for phenol and MB degradation. The enhanced catalytic activity of K-$C_3N_4$ is attributed to the decreased VB position of g-$C_3N_4$ via potassium doping. The separation and immigration of photogenerated carriers under visible light were improved by that as well. This work shed light on the preparation of doping composites with controllable band structures and their application in degradation of organic pollutants.

## Acknowledgments

This work was partly supported by National Basic Research Program of China (973 Program) (2013CB632403), National High Technology Research and Development Program of China (2012AA062701) and Chinese National Science Foundation (20925725 and 21373121).

## Appendix A. Supplementary data

Supplementary data associated with this article can be found, in the online version, at http://dx.doi.org/10.1016/j.apcatb.2014.09.020.

## References

[1] M.R. Hoffmann, S.T. Martin, W. Choi, D.W. Bahnemann, Chem. Rev. 95 (1995) 69–96.
[2] K. Maeda, K. Domen, J. Phys. Chem. Lett. 1 (2010) 2655–2661.
[3] X. Wang, S. Blechert, M. Antonietti, ACS Catal. 2 (2012) 1596–1606.
[4] R. Daghrir, P. Drogui, D. Robert, Ind. Eng. Chem. Res. 52 (2013) 3581–3599.
[5] W. Cui, Y. Liu, L. Liu, J. Hu, Y. Liang, Appl. Catal. A 417–418 (2012) 111–118.
[6] X. Wang, X. Chen, A. Thomas, X. Fu, M. Antonietti, Adv. Mater. 21 (2009) 1609–1612.
[7] X. Wang, K. Maeda, A. Thomas, K. Takanabe, G. Xin, J.M. Carlsson, K. Domen, M. Antonietti, Nat. Mater. 8 (2009) 76–80.
[8] Y. Zheng, J. Liu, J. Liang, M. Jaroniec, S.Z. Qiao, Energ. Environ. Sci. 5 (2012) 6717–6731.
[9] M. Zhang, J. Xu, R. Zong, Y. Zhu, Appl. Catal. B 147 (2014) 229–235.
[10] M. Shalom, S. Inal, C. Fettkenhauer, D. Neher, M. Antonietti, J. Am. Chem. Soc. 135 (2013) 7118–7121.
[11] Y. Zhang, T. Mori, J. Ye, J. Am. Chem. Soc. 132 (2010) 6294–6295.
[12] G.S. Shao, X.J. Zhang, Z.Y. Yuan, Appl. Catal. B 82 (2008) 208–218.
[13] S.C. Yan, Z.S. Li, Z.G. Zou, Langmuir 26 (2010) 3894–3901.
[14] Y. Liu, Y. Lv, Y. Zhu, D. Liu, R. Zong, Y. Zhu, Appl. Catal. B 147 (2014) 851–857.
[15] T. Takata, K. Domen, J. Phys. Chem. C 113 (2009) 19386–19388.
[16] S. Tonda, S. Kumar, S. Kandula, V. Shanker, J. Mater. Chem. A 2 (2014) 6772–6780.
[17] X. Ma, Y. Lv, J. Xu, Y. Liu, R. Zhang, Y. Zhu, J. Phys. Chem. C 116 (2012) 23485–23493.
[18] G. Liu, P. Niu, C. Sun, S.C. Smith, Z. Chen, G.Q. Lu, H.M. Cheng, J. Am. Chem. Soc. 132 (2010) 11642–11648.
[19] M. Calatayud, C. Minot, J. Phys. Chem. C 111 (2007) 6411–6417.
[20] R.C. Haddon, Acc. Chem. Res. 25 (1992) 127–133.
[21] H. Gao, S. Yan, J. Wang, Y.A. Huang, P. Wang, Z. Li, Z. Zou, Phys. Chem. Chem. Phys. 15 (2013) 18077–18084.
[22] M. Wu, J.M. Yan, X. Tang, M. Zhao, Q. Jiang, ChemSusChem 7 (2014) 2654–2658, http://dx.doi.org/10.1002/cssc.201402180.
[23] K.H. Park, B.H. Kim, S.H. Song, J. Kwon, B.S. Kong, K. Kang, S. Jeon, Nano Lett. 12 (2012) 2871–2876.
[24] M.A. Rauf, M.A. Meetani, A. Khaleel, A. Ahmed, Chem. Eng. J. 157 (2010) 373–378.
[25] L. Liu, H. Liu, Y.P. Zhao, Y. Wang, Y. Duan, G. Gao, M. Ge, W. Chen, Environ. Sci. Technol. 42 (2008) 2342–2348.
[26] Y. Liu, Y. Zhu, J. Xu, X. Bai, R. Zong, Y. Zhu, Appl. Catal. B 142–143 (2013) 561–567.
[27] P.V. Zinin, L.C. Ming, S.K. Sharma, V.N. Khabashesku, X. Liu, S. Hong, S. Endo, T. Acosta, Chem. Phys. Lett. 472 (2009) 69–73.
[28] B. Jürgens, E. Irran, J. Senker, P. Kroll, H. Müller, W. Schnick, J. Am. Chem. Soc. 125 (2003) 10288–10300.
[29] J. Xu, Y. Wang, Y. Zhu, Langmuir 29 (2013) 10566–10572.
[30] L. Ge, C. Han, J. Liu, Y. Li, Appl. Catal. A 409–410 (2011) 215–222.
[31] L.W. Zhang, H.B. Fu, Y.F. Zhu, Adv. Funct. Mater. 18 (2008) 2180–2189.
[32] S. Yang, Y. Gong, J. Zhang, L. Zhan, L. Ma, Z. Fang, R. Vajtai, X. Wang, P.M. Ajayan, Adv. Mater. 25 (2013) 2452–2456.
[33] P.D.C. King, T.D. Veal, P.H. Jefferson, J. Zúñiga-Pérez, V. Muñoz-Sanjosé, C.F. McConville, Phys. Rev. B 79 (2009) 035203.